(Received 12 August 2024, Accepted 18 December 2024, Scheduled 27 December 2024)

Implications of Model Complexity in Numerical Studies of Microwave Skin Spectroscopy

Shangyang Shang* and Milica Popović

McGill University, Montreal, Quebec H3A 0E9, Canada

ABSTRACT: Early detection is critical for effective skin cancer treatment. Micro-/millimeter-wave spectroscopy has emerged as a promising noninvasive and cost-effective detection technique. Tissue models are essential in early numerical studies, which typically represent the first step in detector's feasibility assessment. This paper focuses on quantifying implications of numerical model complexity on computational studies of skin spectroscopy. In our comparative numerical studies, we constructed one finger model that follows anatomical structures, as well as its three simplified versions, subjected to simulated measurements with a slim dielectric probe in the 0.5–50 GHz range. Using the finite-element method (FEM) for simulation, we analyzed mesh count to estimate computational cost and return loss variation to assess model reliability. As a result, we reach recommendations for models that optimize computational resources and can yield meaningful information from the standpoint of skin cancer screening. Simplified models are adequate for lower microwave frequencies (< 10 GHz), but at higher frequencies, models with at least three tissue layers (skin, fat, and ligament) are necessary. Modeling smaller tumors requires greater tissue complexity than larger tumors to achieve comparable reliability. Additionally, squamous cell carcinoma (SCC) scenarios demand higher model complexity than basal cell carcinoma (BCC) and melanoma to achieve similar reliability.

1. INTRODUCTION

As the largest organ in the human body, skin provides crucial protection against microorganisms, dehydration, ultraviolet light, and mechanical damage [1]. Skin cancer has historically been the most common type of cancer, posing a significant threat to public health. In North America alone, over 9,500 people are diagnosed with skin cancer daily. In Canada, skin cancers account for approximately one-third of all new cancer cases, with incidence rates on the rise [2]. Skin cancer is broadly classified into two main types: non-melanoma and melanoma. Non-melanoma skin cancer originates in either basal cells or squamous cells of the skin. Basal cell carcinoma (BCC) accounts for over 75% of cases, while squamous cell carcinoma (SCC) makes up 20%. Melanoma, arising in melanocytes — the pigment-producing cells, is less common but more dangerous due to its potential for rapid metastasis.

Early detection is critical for successful skin cancer treatment [3, 4]. For instance, the five-year survival rate for melanoma exceeds 98% at stages 0, I, and II, but drops to 63.6% at stage III. In advanced stage IV melanoma, survival rates plummet to as low as 22.5% [5]. Since the timing of skin cancer appearance and growth is unpredictable, frequent screening is the most reliable method for early diagnosis. Unfortunately, current diagnostic methods fall short in achieving this goal. Typically, dermatologists rely on visual examination [6] and possibly biopsy [7]. Biopsy, an invasive procedure involving tissue removal and subsequent histopathological evaluation under a microscope [8], poses discomfort and anxiety for patients. Given the considerable error rate associated with visual assessment, biopsy is often deemed essential for definitive diagnosis, even in cases where the tissue sample proves to be healthy. This reliance on biopsy highlights the pressing need for a noninvasive tool that can aid dermatologists in characterizing skin lesions with increased confidence.

Recent advancements in micro-/mm-wave technology have demonstrated promise as a noninvasive method for detecting skin cancer. This technology leverages the dielectric contrast between tumor and healthy tissues under microwave scanning [9, 10]. While refining designs and incorporating advanced materials with unique dielectric properties are effective strategies for enhancing detector performance [11–13], an equally important factor is the choice of tissue models used for test and calibration during the development process. This is particularly critical in the early stages, such as simulations and controlled laboratory experiments [14–16]. Nevertheless, existing models often oversimplify geometry and components on a large scale, failing to accurately represent near-skin structures. This simplification can undermine model reliability, especially in regions with complex near-surface anatomy, such as fingers, ears, and toes. However, there is a price to pay for accurate, detailed modeling of human anatomy. Complex models that faithfully replicate the detailed anatomy are usually resource-intensive, requiring substantial computational power for numerical simulations and, in the subsequent stage, complicated and costly fabrication process for controlled, phantom-based experiments.

* Corresponding author: Shangyang Shang (shangyang.shang@mail.mcgill.ca).

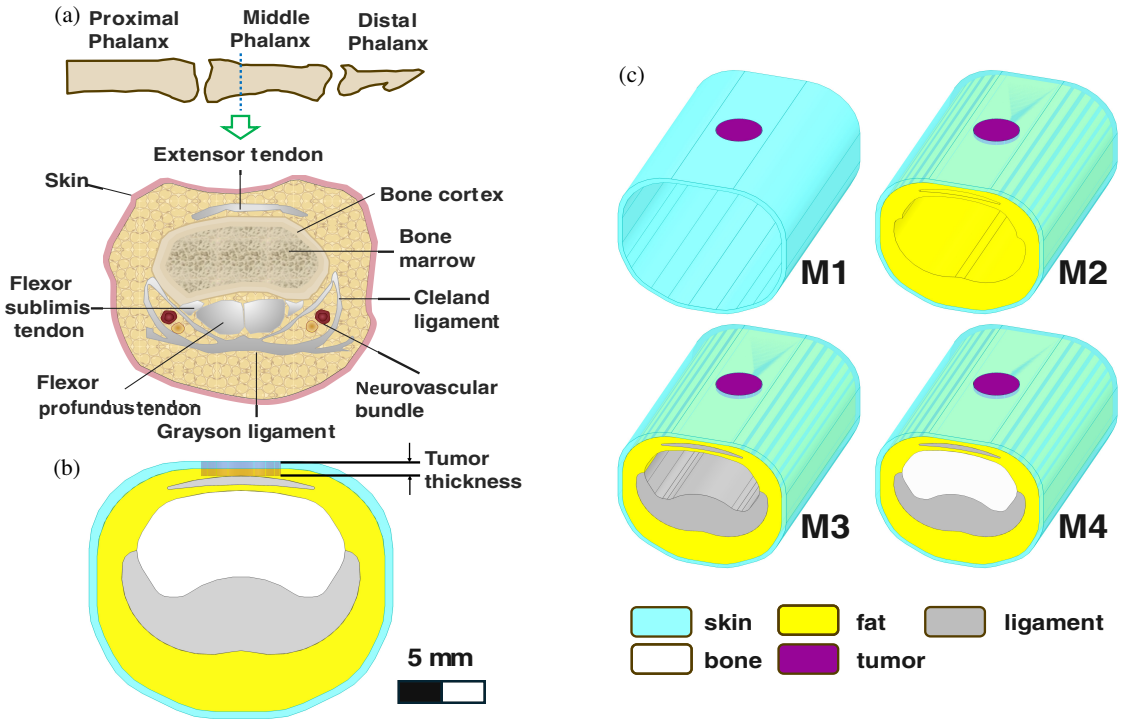

FIGURE 1. (a) Finger anatomy. (b) Cross section of finger model M4, with indicated dimensions. (c) M1, M2, M3 and M4 models, showing the tissues included in each as the model geometry progresses from the single- to the four-tissue complex model.

Building on our initial findings in [17], this work focuses on managing the complexity of tissue models to balance accuracy and efficiency. Specifically, the finger anatomy was selected as the sample subject for several reasons. Firstly, it is particularly vulnerable to cancer formation due to prolonged sunlight exposure and everyday hygiene chemicals [18, 19]. Although the finger comprises only up to 2% of the body's total surface area, it accounts for 10–15% of all reported skin cancer cases [20]. Additionally, the human finger exhibits a complex anatomical structure and composition, rendering it an ideal subject for research involving tissue models at varying levels of complexity.

A finger model was designed in HFSS (High-Frequency Structure Simulator, Ansys) based on the anatomical structure of the mid-phalanx. The model includes four tissue layers: skin, fat, ligament, and bone. Malignant versions of the finger model incorporate three types of skin cancers: basal cell carcinoma (BCC), squamous cell carcinoma (SCC), and melanoma. Additionally, three simplified models were constructed for comparison. The models were evaluated using a slim probe scanning across frequencies from 0.5 GHz to 50 GHz. We quantitatively evaluated model economy through mesh count and assessed model reliability through return loss (S_{11}) differential relative to the reference. Recommendations for model selection are then provided, depending on several factors: frequency, skin cancer type, and tumor size.

The paper is organized as follows. Section 2 outlines the method for building finger models, the approach for assessing model reliability and economy, and the settings in the HFSS simulation experiments. Section 3 presents comparisons of the four finger models in different scenarios, illustrating how selected factors influence model reliability, and provides examples of optimal model complexity selection. Finally, Section 4 summarizes the paper's content and suggests directions for future work.

2. METHOD

2.1. Construction of the Finger Models

Figure 1(a) depicts the anatomical structure of mid-phalanx, featuring the innermost layer composed of bone, surrounded by ligaments, with skin as the outermost layer and the remaining volume filled with fat tissue. Detailed information on the finger components is derived from the magnetic resonance imaging (MRI) scanning results provided by [21], including geometry, relative size, and positioning. Using these data, an accurate numerical finger model was constructed, with the cross-sectional structures depicted in Fig. 1(b). We named this model M4 since it consists of four tissue layers. The dimensions of M4, typical in size, measure 30 mm in length, 19 mm in width, and 17.68 mm in height.

To identify the optimal model complexity for achieving both high reliability and economy in detector development, three

TABLE 1. Composition of the finger models.

Model No.	Skin	Fat	Ligament	Bone
M1	√	×	×	×
M2	√	√	×	×
M3	√	√	√	×
M4	√	√	√	√

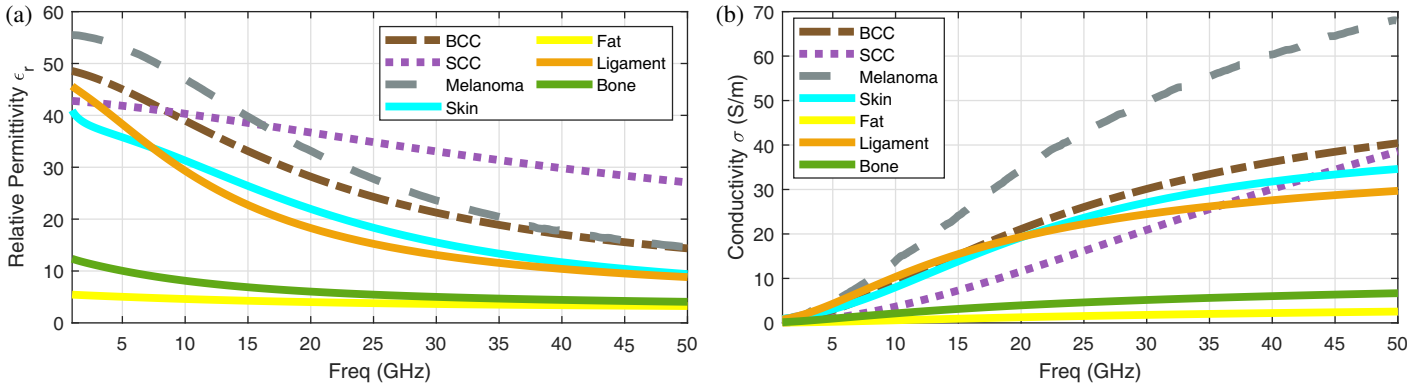

FIGURE 2. The dielectric properties of the healthy and malignant tissues. (a) Relative permittivity. (b) Conductivity.

simplified models were designed by removing tissue layer(s) from M4, as illustrated in Fig. 1(c) and Table 1. The models are named according to the number of tissue layers present: M1 contains only the skin layer; M2 adds a layer of fat tissue; and M3 includes skin, fat, and ligament layers.

2.2. Simulation Settings

Ansys HFSS (version 2023 R2) was chosen to perform the numerical simulations in this study. The HFSS is a commercial finite element method solver developed by Ansys Inc. for electromagnetic (EM) structures. A dielectric slim probe is employed to scan the tissue models by transmitting micro-/mm-wave and receiving the scattered waves. The probe was purchased from Keysight Technologies, Inc., model N1501A. Ref. [22] has demonstrated that the probe can detect small skin cancer tumors in phantom-based experiments. In all scans conducted within this study, the probe was positioned perpendicularly to the tissue models' surface, with the probe tip, characterized by a round cross-section measuring 2.2 mm in diameter, directly contacting the tissue under investigation. For malignant tissues, the probe tip was positioned at the center of the tumor's surface. To mimic the probe measurement environment, the simulations are performed for the frequency range 0.5 GHz–50 GHz, with a step of 0.5 GHz.

In the case of tissue models in a malignant state, three primary types of skin cancers were explored: BCC, SCC, and melanoma. These tumors were placed at the top center of the finger models and were modeled with cylindrical geometries. In Section 3.2.1, tumors were modeled to be 2 mm in diameter (d) and 0.5 mm in thickness (t). Section 3.2.3 explores two lager tumor sizes ($d = 4\,\text{mm}$, $t = 1\,\text{mm}$; $d = 6\,\text{mm}$, $t = 1.5\,\text{mm}$), along with the small one ($d = 2\,\text{mm}$, $t = 0.5\,\text{mm}$), where tumor size, together with tumor type and frequency, is analyzed as factors that determine model complexity selection and identify essential tissue layers. The tumor dimensions in Section 3.2.3 are selected to reflect the tendency of the tumors to progress in both horizontal and vertical directions [23, 24].

We obtained the frequency-dependent dielectric properties of BCC, SCC, and melanoma tumors from [25, 26] and the data of other tissues from "Nello Carrara" Institute of Applied Physics (IFAC), Italy [27]. All the data is illustrated in Fig. 2, where malignant tissues distinguish from healthy tissues in both permittivity and conductivity. Furthermore, it is expected that tumor type will serve as an influential factor, given the significant property differences among BCC, SCC, and melanoma tumors.

2.3. Model Analysis Method

HFSS analyzes electromagnetic (EM) structures by the finite element method (FEM), a well-established numerical technique where the EM structures, i.e., the models, are divided into a number of subsections (finite elements) or meshes [28]. Characterized by the number of meshes, the model economy determines the computational cost of an HFSS computation when other factors, such as the FEM algorithm, frequency, and meshing strategy, remain constant [29–32]. Given the four finger models constructed in this study, it is reasonable to hypothesize that M1 has the highest model economy, as additional layers introduce more elements to help resolve the smaller modeled anatomical structures.

S-parameters are commonly employed as micro-/mm-wave scanning results, as they indicate the relationship between input and output ports [33]. Return loss (S_{11}) was used to describe tissue models response to probe scanning. By closely adhering to the finger's anatomy, M4 and its S_{11} results were established as the reference for evaluating model reliability. By comparing S_{11} differentials from M4 across the 0.5–50 GHz frequency range, the reliability of the simplified models can be quantified.

By jointly analyzing the economy and reliability, while considering the tolerance to design error and available computational resources, it is feasible to identify the optimal model complexity and determine the essential layers that need to be included for meaningful results. Consider an example where developers aim for minimal design error while saving computing resources is secondary. Here, if S_{11} differentials from M4 are negligible across all the simplified models, we can conclude that the skin layer alone suffices. M1 becomes the preferred choice for detector development due to its minimal computing cost. If S_{11} remains consistent across M2, M3, and M4, indicating that both skin and fat layers are essential, M2 should be selected. When M3 emerges as the only simplified model that aligns closely with M4 in terms of S_{11} results, a model comprising skin, fat, and ligament layers is ideal for balancing econ-

omy and reliability. However, if significant S_{11} differences are noted between results of M4 and the simplified models, M4 is identified as the optimal model choice, despite higher computational cost associated with the inclusion of all four tissue layers.

3. RESULTS

3.1. Model Economy: Comparison

In this study, the comparison among finger models regarding model economy is illustrated by the number of meshing elements, as other settings, particularly those related to mesh generation, remain consistent across all models. Fig. 3 demonstrates significant advantages of the simplified models over the complex ones in model economy, with all finger models in a healthy state. Specifically, the M4 model, consisting of 65,018 mesh elements, requires approximately 260 minutes to complete one simulation scan 0.5 GHz–50 GHz. In contrast, the M1 model, with only 14,280 elements, was completed in just 65 minutes using the same computer under the same conditions. M2 and M3, with 30824 and 55171 meshes receptively, require around 140 and 195 minutes per each scan. All computation times are based on simulations performed using an Intel Core i7-12700K processor. These substantial differences in model economy among the finger models underscore the need for minimizing model complexity in skin cancer detector development, provided that the resulting trade-off in simulation accuracy is acceptable.

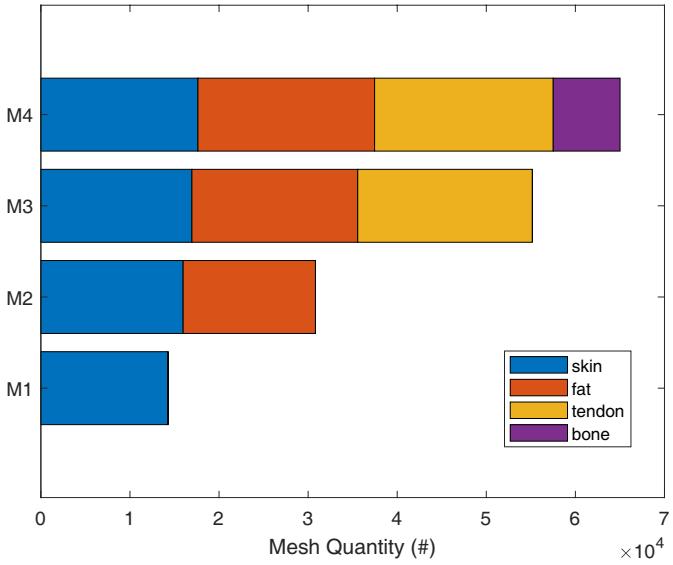

FIGURE 3. M1–M4 model comparison on mesh count.

It is also worth noting that the number of mesh elements for identical layers remains consistent across different models. For instance, the skin layer consistently contains approximately 16,000 mesh elements in all models from M1 to M4. This consistency is a natural outcome of employing the same mesh generation method, which produces nearly identical mesh patterns in terms of volume and geometry within the same layer geometry. The mesh count also provides insight into the significance of each tissue layer in model economy. For instance, the economy gap between M4 and M3 is notably smaller than that between M2 and M1 because the bone layer contributes to the total mesh count with fewer elements than the fat layer.

3.2. Model Reliability: Comparison

3.2.1. The M4 Reference

The return loss at the probe (S_{11}) is used to measure response of numerical models to the probe. When comparing the same model in healthy and malignant states, their responses differ in S_{11} due to variations in dielectric properties. As a result, we hypothesize that S_{11} contrast (ΔS_{11}) can serve as a reliable indicator of the presence of a tumor.

$$\Delta S_{11} = S_{11}(\text{malignant}) - S_{11}(\text{healthy}) \tag{1}$$

One of the key aspects of this study is the analysis of scanning results for the M4 model, which serves as a reference when the reliability of the simplified models is evaluated. Fig. 4(a) shows the S_{11} results on M4 in both healthy and malignant skin tissues. For the malignant one, an early stage of skin cancer is considered, involving a small tumor with a 2-mm diameter and 0.5-mm thickness. Three major skin cancer types, BCC, SCC, and melanoma, are examined. In all four scenarios, S_{11} decreases with increasing frequency. Additionally, clear S_{11} contrasts are observed across the 0.5–50 GHz spectrum between the healthy and malignant models, as well as between the cases with different tumor types. The healthy model shows the overall lower S_{11} because tumors, with higher water content than the healthy tissue, possess higher electrical permittivity. The variations in structure and water content among different tumor types lead to distinct responses. Fig. 4(b) presents the ΔS_{11} results, which further clarify the sharp contrasts between the healthy and malignant cases. The SCC case exhibits the highest contrast across the 0.5–50 GHZ band, with a maximum ΔS_{11} of 3.3 dB at 22.5 GHz. In the cases of BCC and melanoma, higher contrasts are observed in the higher mm-wave frequency band ($>$ 30 GHz). Their maxima are 2.26 dB and 1.68 dB, respectively, both at 50 GHz.

The scanning results on the M4 reference model offering a basis for model comparison. The observed variances on return loss suggest that several factors should be taken into account when evaluating the reliability of a finger model, including frequency, tumor size, and tumor type.

3.2.2. Healthy State

As introduced in Section 2.3, the reliability of the model can be assessed by comparing the differences between a simplified model and the M4 reference in terms of S_{11} results. While a direct comparison, as illustrated in Fig. 5(a), is a straightforward approach, it is insufficient for extracting the precise values of S_{11} differences. Additionally, such a direct comparison does not provide insights into the tendencies of model reliability across different frequencies.

To address this issue, we propose to observe the S_{11} of each of simplified models MX ($X = 1, 2, 3$) and its deviation from the corresponding value of the M4 reference model for each frequency point. Under the hypothesis that model M4 is the most

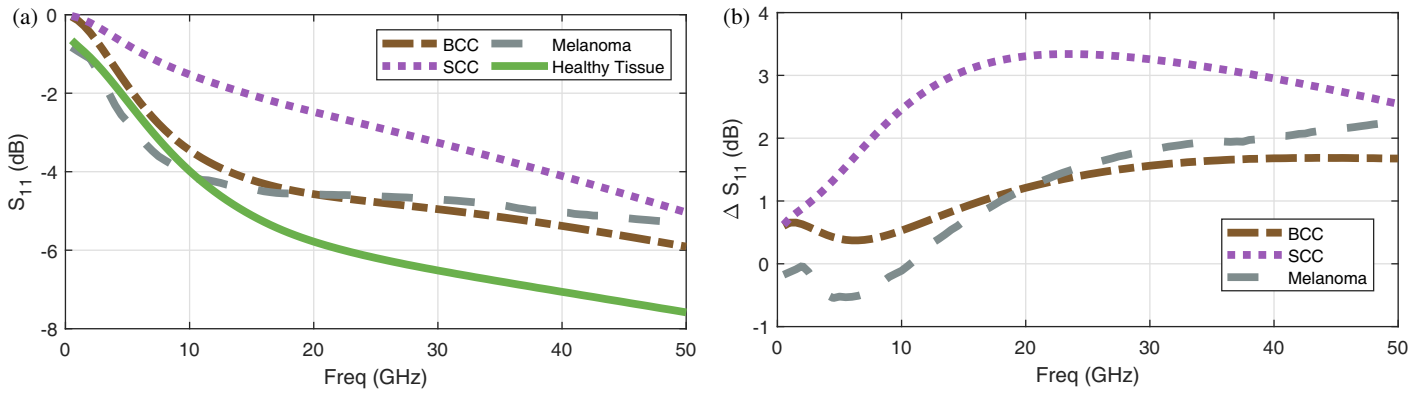

FIGURE 4. (a) The S_{11} simulation results of M4 reference in healthy and malignant condition. (b) The S_{11} contrasts (ΔS_{11}) of results of M4 reference in healthy and malignant condition, obtained by subtracting the healthy response from the one obtained with SCC/BCC/melanoma lesion present.

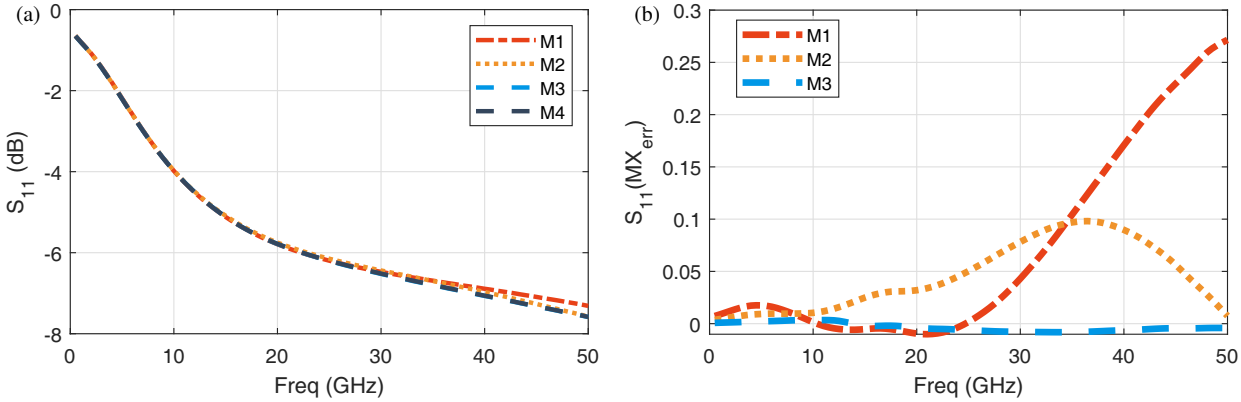

FIGURE 5. (a) Comparison of the four finger models on S_{11} Results. (b) Comparison of M1–M3's model reliability measured by their S_{11} differentials from the M4 reference. All models represent tissue in its healthy state.

anatomically complex and hence can be treated as our reference model, we define this deviation as the error with respect to model M4:

$$S_{11}(\mathrm{MX_{err}}) = S_{11}(\mathrm{MX}) - S_{11}(\mathrm{M4}) \tag{2}$$

where MX denotes a simplified model, and M4 serves as the reference.

Figure 5(b) illustrates the reliability of the simplified models through their S_{11} differential results, in the tumour-free case. M3 shows nearly perfect agreement with M4, with its $S_{11}(\mathrm{M3_{err}})$ value remaining below 0.01 dB across 0.5 GHz–50 GHz. M2's reliability is overall acceptable, as its corresponding error value $S_{11}(\mathrm{M2_{err}})$ differential does not exceed 0.1 dB, but we note that it is frequency-dependent. M1's reliability is acceptable in the 0.5 GHz–25 GHz range but declines drastically at higher frequencies. We note that $S_{11}(\mathrm{M1_{err}})$ is over ten-fold as that of M2 or M3 in the range of 45–50 GHz. The higher S_{11} contrasts at higher frequencies can result from stronger interference effects caused by shorter wavelengths and more pronounced overall dielectric differences among tissue layers.

Consequently, for the healthy models, it can be confirmed, somewhat intuitively, that in the lower frequency range, M1 is generally a suitable choice due to its balance of reliability and computational economy. Therefore, skin appears to be the only essential layer for numerical model construction. However, when high standards and ample resources are allocated to detector design, particularly when the detector's operating frequencies exceed 20 GHz, M3 becomes the preferred model option. In this scenario, the essential layers extend beyond skin to include both fat and ligament.

3.2.3. Malignant State

When coaxial probes are utilized with the aim to characterize visibly abnormal lesions or tumours, most of the power transmitted by the probe is concentrated around the probe tip, owing to the frequency-dependent losses and the short penetration depth of electromagnetic waves in skin tissue [34]. This penetration depth ranges from 0.5 mm to 50 mm across the 0.5–50 GHz frequency range [27], when taking into account the allowed power level limits set by safety policy considerations. Consequently, the area effectively detected by the probe is limited, typically spanning only several millimeters beyond the probe's cross-sectional area.

Therefore, tumor size is a crucial factor in the reliability comparison of malignant finger models. For the purpose of this study, three levels of cylindrical tumor sizes were considered:

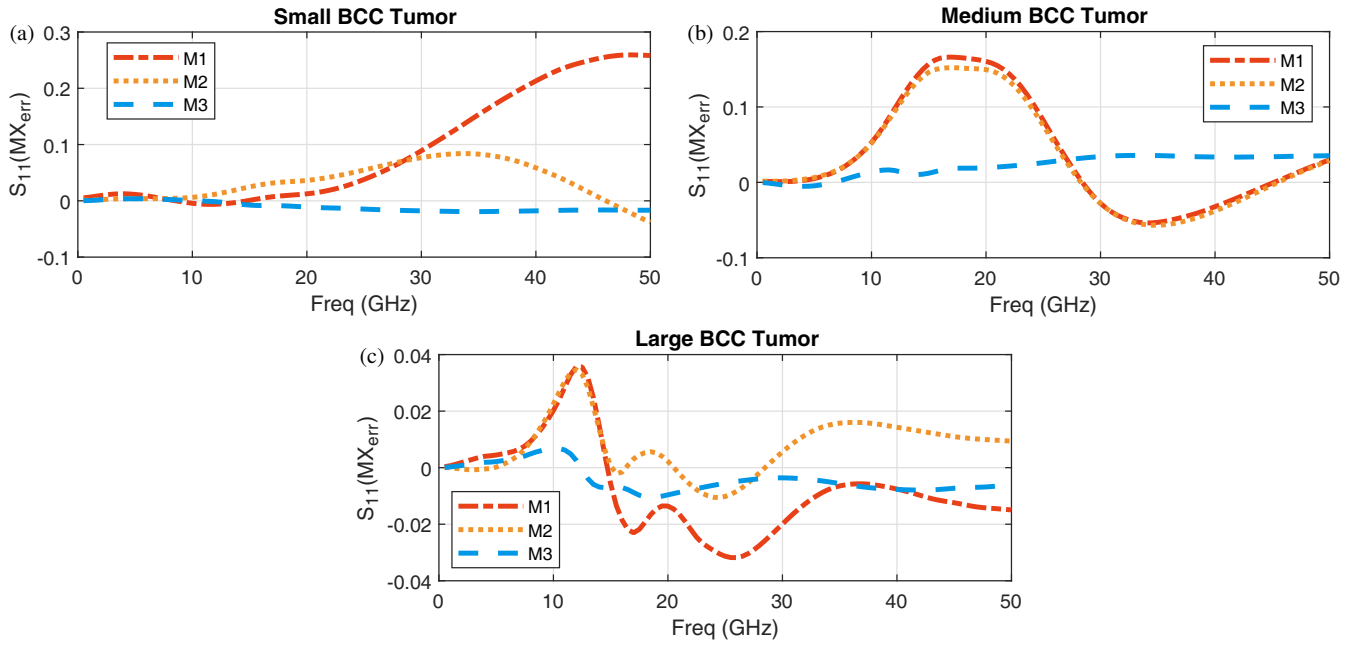

FIGURE 6. M1–M3's model reliability measured by their S_{11} differentials from the M4 reference. All models are malignant BCC with differently sized tumours. (a) Small, (b) medium and (c) large BCC tumor.

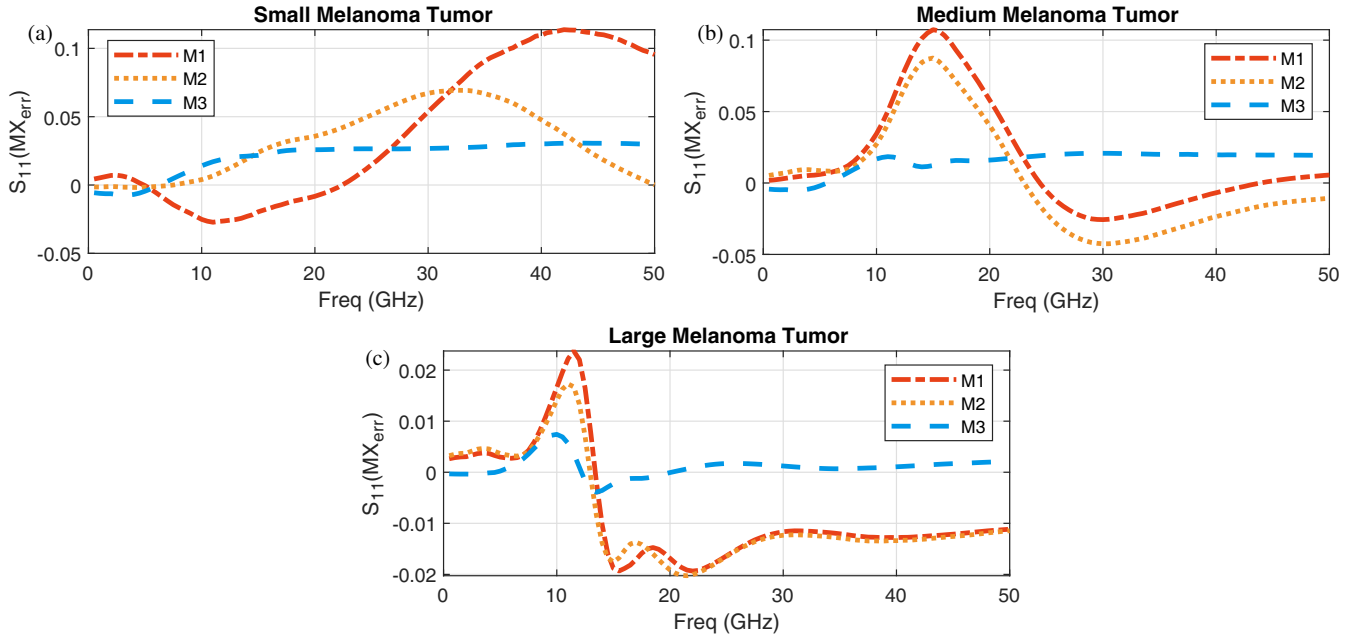

FIGURE 7. M1–M3's model reliability measured by their S_{11} differentials from the M4 reference. All models are malignant melanoma with differently sized tumors. (a) Small, (b) medium and (c) large melanoma tumor.

small (diameter: 2 mm, thickness: 0.5 mm), medium (diameter: 4 mm, thickness: 1 mm), and large (diameter: 6 mm, thickness 1.5 mm). We note, importantly, that the probe tip diameter measures 2.2 mm. The rationale behind the increasing tumor thicknesses is that tumors typically grow in both radial and thickness dimensions as the skin cancer advances. Given the variation of the frequency-dependent dielectric properties among BCC/SCC/melanoma tumors, tumor type and frequency become additional factors that should be considered, along with tumor size, in malignant finger model comparison.

Figure 6 reveals the $S_{11}(\mathrm{MX_{err}})$ values when all the models now have added malignant lesion, a BCC tumor, of varying size. It is shown that the $S_{11}(\mathrm{MX_{err}})$ universally decreases with tumor size. These results suggest that, with smaller tumors, finger model complexity plays an important role at higher frequencies. Conversely, a larger tumor that occupies, and exceeds, the entire probe sensing region can overshadow the differences in

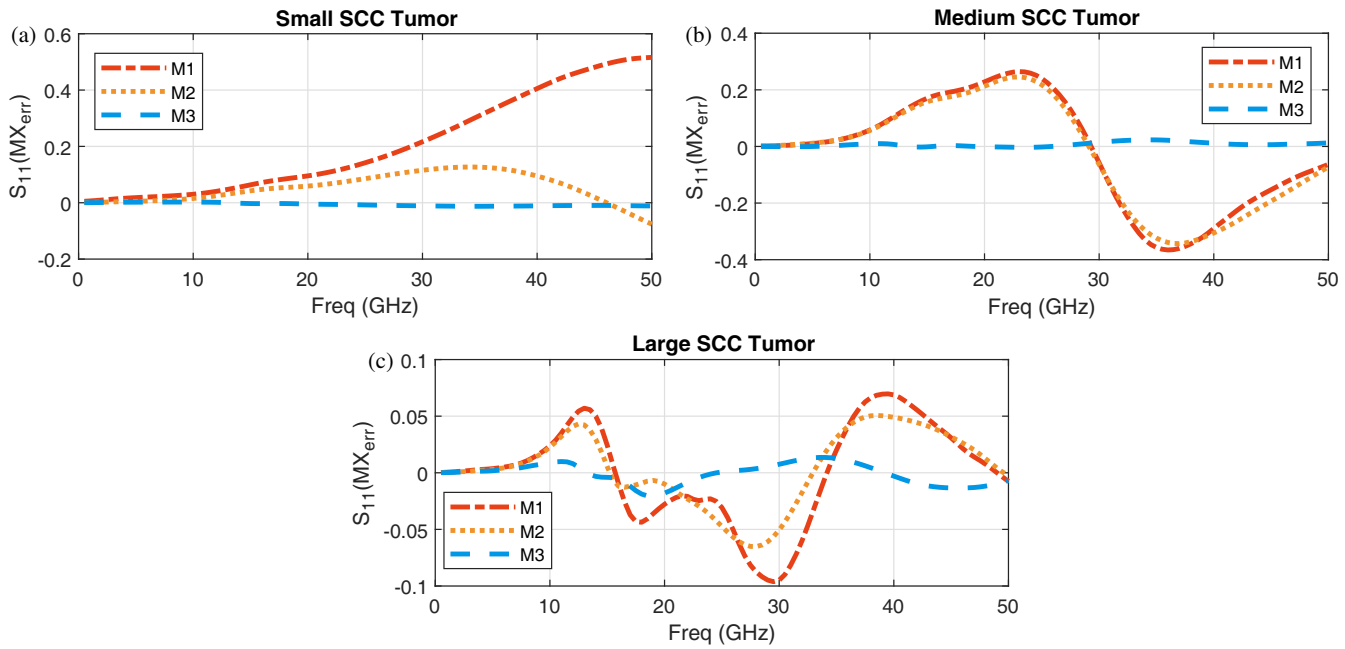

FIGURE 8. M1–M3's model reliability measured by their S_{11} differentials from the M4 reference. All models are malignant SCC with differently sized tumors. (a) Small, (b) medium and (c) large SCC tumor.

tissue components through high loss. As for frequency dependence, we note that the $S_{11}(\mathrm{MX_{err}})$ shows different variation, and depends on the the tumor size relative to the probe and the tissue discontinuities around it. These results suggest that, for lower frequencies, regardless of the BCC tumor size, M1 and M2 are sufficient in complexity, while for frequencies above 10 GHz, the complexity of M3 is necessary for reliable results that approach those of the most complex model, M4.

We proceed with the same analysis of results for melanoma and SCC tumours. As depicted in Figs. 7 and 8, tumor size and frequency influence $S_{11}(\mathrm{MX_{err}})$, our measure for model reliability, in a manner similar to the BCC cases. Similar conclusions can be drawn as well. First, the $S_{11}(\mathrm{MX_{err}})$ values decrease with increasing tumor size and almost vanish in the large-tumor cases, where the entire probe detection area is occupied by the malignant tissue exclusively. Second, the reliability of M1 and M2 models with included small tumors is acceptable up to 10 GHz. Third, when dealing with larger SCC/melanoma tumors, M1 appears to be the optimal choice in terms of both economy and reliability. In cases with the small tumors, increasing model complexity (M2 or M3) is necessary. Finally, tumor type demonstrates its critical role in model reliability evaluation: the dielectric properties of SCC, BCC, and melanoma are sufficiently different to necessitate specification of tumour type within the models.

It is also worth noting that $S_{11}(\mathrm{M3_{err}})$ never exceeds 0.03 dB at all tumor types, sizes, and frequencies, indicating that M3 is always a robust and reliable choice when aiming to universally precise tumor detectors. Accordingly, skin, fat, and tissue are the essential tissues to be included in numeral models of the human finger anatomy.

4. CONCLUSION AND DISCUSSION

In this study, we have introduced a quantitative method to evaluate the economy and reliability of tissue models used in skin cancer detector development. By analyzing mesh count for computational economy and scan differentials from a reference, most complex, model for reliability, we aimed to identify the optimal complexity for tissue models.

We demonstrated our approach using a finger model as an example. This included a detailed reference model based on anatomical structures and three simplified versions, all tested with a slim probe across a frequency range of 0.5 GHz to 50 GHz. Our findings revealed that the economy of the models, measured by mesh count, significantly decreases as the model complexity increases. Regarding reliability, three key factors were found to be important: frequency, tumor type, and tumor size. Simplified models are generally acceptable in the lower microwave band (< 10 GHz), while models involving at least skin, fat and ligament are required for higher-frequencies. Smaller tumor modeling required higher tissue complexity than that of larger tumors, for comparably reliable results. Compared with BCC and melanoma, higher model complexity is required in the SCC scenarios to achieve the same level of model reliability.

Future work will focus on developing tissue models for a broader range of body sites and examining the impact of model complexity on various types of skin cancer detectors, including low-profile options based on antennas. Additionally, the theories and conclusions drawn from this research will be validated through phantom-based experiments.

REFERENCES

[1] Lacy, K. and W. Alwan, "Skin cancer," *Medicine (United Kingdom)*, Vol. 41, No. 7, 402–405, Jul. 2013.

[2] Siegel, R. L., K. D. Miller, N. S. Wagle, and A. Jemal, "Cancer statistics, 2023," *CA: A Cancer Journal for Clinicians*, Vol. 73, No. 1, 17–48, 2023.

[3] Ersser, S. J., A. Effah, J. Dyson, I. Kellar, S. Thomas, E. McNichol, E. Caperon, C. Hewitt, and A. J. Muinonen-Martin, "Effectiveness of interventions to support the early detection of skin cancer through skin self-examination: A systematic review and meta-analysis," *British Journal of Dermatology*, Vol. 180, No. 6, 1339–1347, 2019.

[4] Jerant, A. F., J. T. Johnson, C. D. Sheridan, and T. J. Caffrey, "Early detection and treatment of skin cancer," *American Family Physician*, Vol. 62, No. 2, 357–368, 2000.

[5] Petrie, T., R. Samatham, A. M. Witkowski, A. Esteva, and S. A. Leachman, "Melanoma early detection: Big data, bigger picture," *J. of Invest. Dermatol.*, Vol. 139, No. 1, 25–30, 2019.

[6] Massone, C., A. D. Stefani, and H. P. Soyer, "Dermoscopy for skin cancer detection," *Current Opinion in Oncology*, Vol. 17, No. 2, 147–153, 2005.

[7] Rosendahl, C., P. Tschandl, A. Cameron, and H. Kittler, "Diagnostic accuracy of dermatoscopy for melanocytic and nonmelanocytic pigmented lesions," *Journal of the American Academy of Dermatology*, Vol. 64, No. 6, 1068–1073, 2011.

[8] Nault, A., C. Zhang, K. Kim, S. Saha, D. D. Bennett, and Y. G. Xu, "Biopsy use in skin cancer diagnosis: Comparing dermatology physicians and advanced practice professionals," *JAMA Dermatology*, Vol. 151, No. 8, 899–902, 2015.

[9] Cook, H. F., "The dielectric behaviour of some types of human tissues at microwave frequencies," *British Journal of Applied Physics*, Vol. 2, No. 10, 295, 1951.

[10] Schwan, H. P., "Electrical property of tissues and cells," *Advance in Biological & Medical Physics*, Vol. 5, 147–207, 1957.

[11] Zhang, L., Z. Chen, K. Zhang, L. Wang, H. Xu, L. Han, W. Guo, Y. Yang, C.-N. Kuo, C. S. Lue, *et al.*, "High-frequency rectifiers based on type-II Dirac fermions," *Nature Communications*, Vol. 12, No. 1, 1584, 2021.

[12] Vobornik, I., A. B. Sarkar, L. Zhang, D. W. Boukhvalov, B. Ghosh, L. Piliai, C.-N. Kuo, D. Mondal, J. Fujii, C. S. Lue, *et al.*, "Kitkaite NiTeSe, an ambient-stable layered dirac semimetal with low-energy type-ii fermions with application capabilities in spintronics and optoelectronics," *Advanced Functional Materials*, Vol. 31, No. 52, 2106101, 2021.

[13] Politano, A., L. Viti, and M. S. Vitiello, "Optoelectronic devices, plasmonics, and photonics with topological insulators," *APL Materials*, Vol. 5, No. 3, 035504, 2017.

[14] Arab, H., L. Chioukh, M. D. Ardakani, S. Dufour, and S. O. Tatu, "Early-stage detection of melanoma skin cancer using contactless millimeter-wave sensors," *IEEE Sensors Journal*, Vol. 20, No. 13, 7310–7317, 2020.

[15] Töpfer, F., S. Dudorov, and J. Oberhammer, "Millimeter-wave near-field probe designed for high-resolution skin cancer diagnosis," *IEEE Transactions on Microwave Theory and Techniques*, Vol. 63, No. 6, 2050–2059, 2015.

[16] Mirbeik-Sabzevari, A. and N. Tavassolian, "Tumor detection using millimeter-wave technology: Differentiating between benign lesions and cancer tissues," *IEEE Microwave Magazine*, Vol. 20, No. 8, 30–43, 2019.

[17] Shang, S. and M. Popović, "Finger models: Example of complex geometry in investigations on microwave skin cancer diagnosis," in *2023 IEEE MTT-S International Microwave Biomedical Conference (IMBioC)*, 154–156, Leuven, Belgium, Sep. 2023.

[18] Ilyas, E. N., C. F. Leinberry, and A. M. Ilyas, "Skin cancers of the hand and upper extremity," *The Journal of Hand Surgery*, Vol. 37, No. 1, 171–178, 2012.

[19] Gallagher, R. P., C. D. Bajdik, S. Fincham, G. B. Hill, A. R. Keefe, A. Coldman, and D. I. McLean, "Chemical exposures, medical history, and risk of squamous and basal cell carcinoma of the skin." *Cancer Epidemiology, Biomarkers & Prevention: A Publication of the American Association for Cancer Research, Cosponsored by the American Society of Preventive Oncology*, Vol. 5, No. 6, 419–424, 1996.

[20] Maciburko, S. J., W. A. Townley, K. Hollowood, and H. P. Giele, "Skin cancers of the hand: A series of 541 malignancies," *Plastic and Reconstructive Surgery*, Vol. 129, No. 6, 1329–1336, 2012.

[21] Van Zwieten, K. J., K. P. Schmidt, P. Adriaensens, O. E. Piskun, and S. A. Varzin, "Anatomical evidence supports recent hypothesis on the pathogenesis of Dupuytren's contracture," *Клиническая Патофизиология*, Vol. 3, 71–78, 2019.

[22] Boparai, J. and M. Popović, "Development and characterization of skin phantoms at microwave frequencies," *IEEE Journal of Electromagnetics, RF and Microwaves in Medicine and Biology*, Vol. 6, No. 3, 296–304, 2022.

[23] Tchinov, R., J. Boparai, O. Miller, Y. Jallouli, and M. Popović, "Microwave spectroscopy of melanoma progression model," in *2023 17th European Conference on Antennas and Propagation (EuCAP)*, 1–4, Florence, Italy, Mar. 2023.

[24] Beer, J., L. Xu, P. Tschandl, and H. Kittler, "Growth rate of melanoma in vivo and correlation with dermatoscopic and dermatopathologic findings," *Dermatology Practical & Conceptual*, Vol. 1, No. 1, 59–67, 2011.

[25] Mirbeik-Sabzevari, A., R. Ashinoff, and N. Tavassolian, "Ultra-wideband millimeter-wave dielectric characteristics of freshly excised normal and malignant human skin tissues," *IEEE Trans. on Biomedical Engineering*, Vol. 65, No. 6, 1320–1329, 2017.

[26] Mohammed, B. J., S. A. R. Naqvi, M. Manoufali, K. Bialkowski, and A. M. Abbosh, "Changes in epidermal dielectric properties due to skin cancer across the band 1 to 50 GHz," in *2018 Australian Microwave Symposium (AMS)*, 77–78, Brisbane, QLD, Australia, Feb. 2018.

[27] IFAC-CNR, "Calculation of the dielectric properties of body tissues in the frequency range 10 Hz–100 GHz," http://niremf.ifac.cnr.it/tissprop/htmlclie/htmlclie.php, 2024.

[28] Cendes, Z., "The development of HFSS," in *2016 USNC-URSI Radio Science Meeting*, 39–40, Fajardo, PR, USA, Jun. 2016.

[29] Okereke, M. and S. Keates, "Finite element mesh generation," *Finite Element Applications: A Practical Guide to the FEM Process*, 165–186, 2018.

[30] Shaowu Yuchi, H., V. R. Joseph, and C. F. J. Wu, "Design and analysis of multifidelity finite element simulations," *Journal of Mechanical Design*, Vol. 145, No. 6, 061703, 2023.

[31] Sumithra, P. and D. Thiripurasundari, "Review on computational electromagnetics," *Advanced Electromagnetics*, Vol. 6, No. 1, 42–55, 2017.

[32] Ansys HFSS, "Solvers, meshing and solution setup in ansys HFSS 3d layout — Lesson 3," Ansys Innovation Courses, 2021.

[33] Mehrotra, P., B. Chatterjee, and S. Sen, "EM-wave biosensors: A review of RF, microwave, mm-wave and optical sensing," *Sensors*, Vol. 19, No. 5, 1013, 2019.

[34] La Gioia, A., S. Salahuddin, M. O'Halloran, and E. Porter, "Quantification of the sensing radius of a coaxial probe for accurate interpretation of heterogeneous tissue dielectric data," *IEEE Journal of Electromagnetics, RF and Microwaves in Medicine and Biology*, Vol. 2, No. 3, 145–153, 2018.